Journal of Materials Chemistry B

PAPER

View Article Online
View Journal | View Issue

Cite this: J. Mater. Chem. B, 2014, 2, 6669

A 3D origami electrochemical immunodevice based on a Au@Pd alloy nanoparticle-paper electrode for the detection of carcinoembryonic antigen†

Li Li,[a] Chao Ma,[a] Qingkun Kong,[a] Weiping Li,[a] Yan Zhang,[a] Shenguang Ge,[b] Mei Yan[b] and Jinghua Yu*[a]

Received 17th July 2014
Accepted 11th August 2014

DOI: 10.1039/c4tb01178c

www.rsc.org/MaterialsB

Herein, a novel 3D microfluidic paper-based electrochemical (EC) immunodevice (μ-PEI) for sensitive detection of carcinoembryonic antigen (CEA) was developed. Au@Pt core–shell nanoparticles (NPs), with high conductivity, large surface area, and synergistic electronic effects, were not only used as carriers of secondary antibodies, methylene blue (MB) redox probes and glucose oxidase but also catalyzed the EC reaction of MB, thus amplifying the EC signal of MB in the presence of glucose. In addition, using a novel Au@Pd alloy NP modified porous paper working electrode as the biosensor platform could not only enhance the surface area to immobilize antibodies but also catalyze the reduction of hydrogen peroxide, which further amplified the detection response. On the basis of the considerably amplified EC signal and the sandwich-type format, the EC immunosensor has a sensitive response to CEA in a linear range of 1.0 pg mL^{-1}–100 ng mL^{-1} with a detection limit of 0.4 pg mL^{-1}. Additionally, this 3D μ-PEI showed satisfactory reproducibility, selectivity and stability.

1 Introduction

Paper, as one of the most important inventions, is already utilized extensively as a platform in analytical and clinical chemistry.[1] As an analytical support, paper, being relatively cheap, abundant, disposable and easy to use, store, and transport, has excellent chemical compatibility with many applications.[2] Since the first patterned paper was proposed by Martinez *et al.*, microfluidic paper-based analytical devices (μ-PADs), which combine the simplicity and low-cost of paper strip tests and the complexity of the conventional lab-on-chip devices, have never attracted as much attention as they do now.[3] Importantly, μ-PADs are easily fabricated in the bulk using wax-printing and this method has been found effective in the production of μ-PADs at minute cost.[4] Inspired by this simple technique, some groups have paid great efforts to the development of μ-PADs, including fabrication methods, functionalizations or modifications, and analytical methods on μ-PADs.[5–7]

For practical clinical application, now tremendous efforts have been focused on developing low-cost and portable methods. The conventional analytical methods, such as, fluorescence,[8] chemiluminescence,[9] electrochemiluminescence[10] and electrochemistry,[11] have been devoted to realizing sensitive detection. Among them, electrochemical (EC) methods,[12] which distinguish themselves by convenient miniaturization and integration, easy signal quantification, simple instrumentation, and low cost of the entire assay, can be ideal alternatives.

Bimetallic nanoparticles (NPs) are attractive materials owing to their novel optical, catalytic, electronic, and magnetic properties which are distinctly different from those of their monometallic counterparts.[13–17] As in the case of monometallic NPs, these properties can be controlled by tuning the size and shape of the NPs. Accordingly, bimetallic NPs (core–shell and alloy) with a well-controlled morphology may even show optimized physicochemical properties.[18–20] In this work, Au@Pt core–shell NPs were used as carriers for electroactive and biocompatible cationic dye methylene blue (MB) attachment (MB/Au@Pt) by electrostatic interaction. The prepared Au@Pt NPs present distinct synergetic characteristics due to the strain and electronic effects between the different components, where Pt showed specific electrocatalytic activity and long-term stability, while Au showed both high conductivity and biocompatibility.[21] On the other hand, Au@Pd alloy NPs prepared *via* a seed-mediated synthetic method by using H_2PdCl_4 and $HAuCl_4$ as metal sources and L-ascorbic acid (AA) as a reductant showed dramatically enhanced catalytic activity, and have been widely studied because of their excellent catalytic efficiencies for a variety of chemical reactions.[22] Here, an interconnected Au@Pd alloy NP layer was grown on the surfaces of cellulose fibers from Au NP seeds in the paper sample zone of the paper working

[a]Key Laboratory of Chemical Sensing & Analysis in Universities of Shandong, University of Jinan, Jinan 250022, China. E-mail: ujn.yujh@gmail.com; Tel: +86-531-82767161

[b]Shandong Provincial Key Laboratory of Preparation and Measurement of Building Materials, University of Jinan, Jinan 250022, China

† Electronic supplementary information (ESI) available. See DOI: 10.1039/c4tb01178c

electrode (PWE) to fabricate novel Au@Pd–PWE on a 3D EC paper-based device. The sensitivity of Au@Pd–PWE was much higher than that of a bare one (unmodified PWE) because of the high ratio of surface area to weight (9.5 $m^2 g^{-1}$)[23] and the porous structure of paper as well as the high conductivity of Au@Pd NPs. Taking into consideration the above advantages, it would be an effective way to integrate Au@Pd–PWE with MB/Au@Pt hybrids as magnified elements for constructing a sensitive EC biosensor.

In this paper, we described the construction of a sensitive sandwich-type EC immunosensor for carcinoembryonic antigen (CEA) detection by combining a microfluidic paper-based device. Greatly enhanced sensitivity for this microfluidic paper-based EC immunodevice (μ-PEI) was based on a dual-signal amplification strategy. The novel Au@Pd–PWE served as an immunosensing platform, which could not only facilitate the electron transfer and provide a large accessible surface area for the immobilization of the antibody but also catalyze the reduction of H_2O_2 to enhance the EC signals. MB/Au@Pt hybrids with excellent EC activity and excellent electrocatalytic activity, which were selected as redox probes, improved the signal response. With the aid of a simple home-made device-holder, the proposed method showed high sensitivity and wide linear detection response for CEA, indicating great potential for point-of-care diagnostics.

2 Experimental section

2.1 Materials

Human CEA, mouse monoclonal capture antibodies ($McAb_1$) and signal antibodies ($McAb_2$) were purchased from Linc-Bio Science Co. Ltd. (Shanghai, China). The clinical serum samples were purchased from Shandong Tumor Hospital. Bovine serum albumin (BSA) and glucose oxidase (GOx) were obtained from Sigma-Aldrich Chemical Co. (USA). Hydrogen hexachloroplatinate(IV) hydrate ($H_2PtCl_6 \cdot 6H_2O$), tetrachloropalladate acid (H_2PdCl_4), MB and AA were obtained from Aldrich. Carbon ink (ELECTRODEDAGPF-407C) and silver/silver choride (Ag/AgCl) ink (ELECTRODAG7019 (18DB19C)) were purchased from Acheson (Germany). Chloroauric acid ($HAuCl_4 \cdot 4H_2O$) was obtained from Shanghai Reagent Company (Shanghai, China). All other reagents were of analytical grade and used as received. Ultrapure water obtained from a Millipore water purification system (>18.2 MΩ cm, Milli-Q, Millipore) was used in all assays and solutions. Phosphate-buffered saline (PBS, 10.0 mM) with different pH values was prepared by mixing the stock solutions of KH_2PO_4 and Na_2HPO_4. PBS (0.1 M, pH 7.4) containing 1.5 mM glucose was used as the electrolyte in the measuring system. The washing buffer was PBS (pH 7.4, 10.0 mM) containing 0.05% (w/v) Tween-20. PBS (pH 7.4, 10.0 mM) containing 0.5% (w/v) BSA and 0.5% (w/v) casein was used as blocking solution. Whatman chromatography paper #1 (20.0 cm × 20.0 cm) (pure cellulose paper) was obtained from GE Healthcare Worldwide (Pudong Shanghai, China) and used with further adjustment of size.

2.2 Apparatus

Ultraviolet-visible (UV-vis) absorption spectra were recorded on a UV-2550 spectrophotometer (Shimadzu, Japan). Scanning electron microscopy (SEM) images were obtained using a QUANTA FEG 250 thermal field emission scanning electron microscope (FEI Co., USA). Energy dispersive X-ray spectroscopy (EDS) was carried out using an X-MAX50 energy dispersive spectrometer (Oxford, UK). Transmission electron microscopy (TEM) images were obtained from a JEOL JEM-1400 microscope (Japan). The phase characterization was performed by X-ray diffraction (XRD) using a D8 advance diffractometer system equipped with Cu Kα radiation (Bruker Co., Germany). Electrochemical impedance spectroscopy (EIS) was performed on an IM6x electrochemical station (Zahner, Germany).

2.3 Preparation of the 3D paper-based EC device

The fabrication procedure of the 3D paper-based EC device was similar to our previous work[24] and the detailed procedure is described in the ESI.† As shown in Scheme S1,† this 3D paper-based EC device, comprised of two circular paper working zones, was fabricated through wax-printing. After folding at the predefined fold line (1 mm in width), the three screen-printed electrodes (working electrode, reference electrode, and counter electrode) would be connected once the paper EC cell was filled with solution (40 μL).

2.4 Synthesis of signal labels

Firstly, Au NPs with a diameter of 13 nm were produced by reducing $HAuCl_4 \cdot 4H_2O$ with citric acid at 100 °C for 1.5 h.[25] Secondly, 1% H_2PtCl_6 (20 mM) was dispersed in Au NP solution. The mixture was allowed to react with vigorous stirring for 10 min at 100 °C. Afterwards, 10 mL of AA solution (100 mM) was dropped into the mixture and heated for 20 min to obtain Au@Pt NP solution. Subsequently, the MB/Au@Pt hybrids were prepared as follows: 2 mL of Au@Pt NP solution was mixed with 2 mL of MB solution (1 mM) and stirred vigorously for 24 h for MB attachment. After washing with water, MB/Au@Pt hybrids were obtained. Finally, the GOx/$McAb_2$/MB/Au@Pt bioconjugates were prepared as follows: 1 mL of 20 μg mL^{-1} $McAb_2$ was added into the solution of MB/Au@Pt hybrids for $McAb_2$ attachment. The mixed suspension was stirred at 4 °C for 12 h. 1.0 mL of GOx (1.0 mg mL^{-1}) was added into the $McAb_2$/MB/Au@Pt suspension with gentle stirring at 4 °C for 8 h to block the surface nonspecific sites. The GOx/$McAb_2$/MB/Au@Pt bioconjugates were stored at 4 °C before use.

2.5 Preparation of the novel Au@Pd–PWE

The novel Au@Pd–PWE was fabricated through growth of an Au@Pd alloy NP layer on the surfaces of cellulose fibers in the paper sample zone of PWE to enhance the conductivity and enlarge the effective surface area of PWE. The fabrication procedures of the Au@Pd–PWE are described as follows: Firstly, 15.0 μL of Au NP seed solution was dropped into the paper sample zone of PWE. Then the paper-based device was equilibrated at room temperature for 1 h. After rinsing with water

thoroughly according to the method in our previous work[26] to remove loosely bound Au NP seeds, the Au NP seeded PWE was added into prepared growth solution containing $HAuCl_4$ (10 mM) and H_2PdCl_4 (20 mM). Then, AA solution (100 mM) was added quickly under gentle shaking. Finally, the resulting Au@Pd–PWE was washed with water thoroughly and dried at room temperature for 30 min.

2.6 Fabrication of μ-PEI

In brief, $McAb_1$ (4.0 μL, 20.0 μg mL^{-1}) was applied to the Au@Pd–PWE and incubated for 40 min. Subsequently, physically absorbed excess $McAb_1$ was washed out with washing buffer. A drop of 4.0 μL of blocking solution was then applied to the Au@Pd–PWE and incubated for 30 min at room temperature to block nonspecific adsorption sites. After another washing with washing buffer, the resulting μ-PEI was obtained and stored at 4 °C in a dry environment prior to use.

2.7 EC assay procedure

As shown in Scheme 1, the μ-PEI was incubated with 4.0 μL of CEA standard solution with different concentrations for 170 s at room temperature, followed by washing with washing buffer. Then the μ-PEI was further incubated with 4.0 μL of the designed bioconjugate for 170 s at room temperature. After another washing with washing buffer, the μ-PEI was integrated with a home-made device-holder. Therefore, the μ-PEI was fixed and connected to the EC workstation. The EC measurements were carried out in 40 μL of PBS (pH 7.4) containing 1.5 mM glucose and the amperometric responses of the immunosensor were recorded by differential pulse voltammetry (DPV) with a pulse amplitude of 50 mV and a pulse width of 50 mS from −0.6 to 0 V.

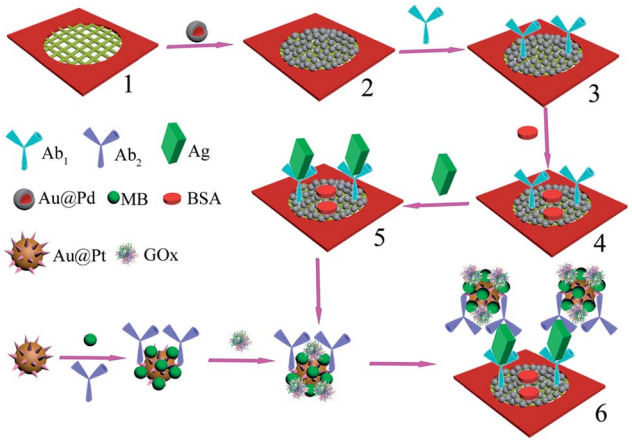

Scheme 1 The schematic representation of the fabrication procedure for the 3D origami ECL immunodevice. (1) Bare PWE; (2) Au@Pd–PWE; (3) after immobilization with $McAb_1$; (4) after blocking with BSA; (5) after capture and washing; (6) after incubation with signal antibodies and washing.

3 Results and discussion

3.1 Characterization of Au@Pd–PWE

The bare paper working zone with a high surface area could provide a fine adsorption capability for the Au NP seeds.[27] As shown in Fig. S1,† there was no apparent structural and surface difference between the bare (Fig. S1A†) and the Au NP seeded cellulose fibers (Fig. S1B†) due to the small particle size of Au NP seeds. As the growth time increased, the Au@Pd NPs were rapidly enlarged by incubating in the growth solution. Finally, as shown in Fig. 1A–C, a continuous and dense conducting Au@Pd layer with interconnected Au@Pd NPs on the cellulose fiber surface in the paper sample zone was observed after 10 min of growth. The elemental compositions of Au@Pd–PWE were analyzed by EDS (the inset in Fig. 1B) and the EDS analyses showed that the sample consisted of C, Au and Pd elements. The size distribution of Au@Pd NPs is shown in the inset in Fig. 1C. The crystal structures of Au@Pd NPs were characterized by XRD. Fig. 1D shows that one representative diffraction peak appeared at 22.8°, which corrresponded to the cellulose (002) plane (JCPDS 03-0289). Another four reflections appeared at 39.6, 45.6, 66.6, and 79.8°, which were coincidently located between Au (reference code: 00-004-0784) and Pd (reference code: 00-005-0681) and could be indexed as the (111), (200), (220), and (311) reflections of the face-centered cubic Au@Pd NPs, indicating the successful fabrication of Au@Pd–PWE.[28,29]

3.2 Characterization of GOx/$McAb_2$/MB/Au@Pt bioconjugates

Fig. 2A, B show SEM and TEM images of Au@Pt NPs, respectively. The Au@Pt NPs were spherical and uniform with an average size of ~20 nm (Fig. 2A). Fig. 2B shows that the core–shell structures of the Au@Pt NPs were successfully prepared. EDS (Fig. 2C) analyses showed that the sample consisted of Au and Pt elements, indicating the formation of Au@Pt NPs. The GOx/$McAb_2$/MB/Au@Pt bioconjugates were further characterized using UV-vis spectroscopy. As shown in Fig. 2D, a visible

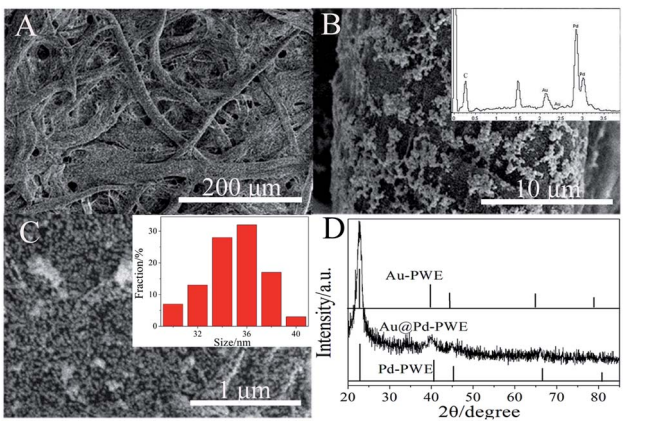

Fig. 1 (A–C) Enlarged Au@Pd on the surfaces of cellulose fibers in the paper sample zone of PWE under different magnifications after 10 min of growth; (D) XRD patterns of the Au–PWE; Pd–PWE; Au@Pd–PWE. Inset in (B and C): EDS of Au@Pd–PWE and size distributions of Au@Pd NPs.

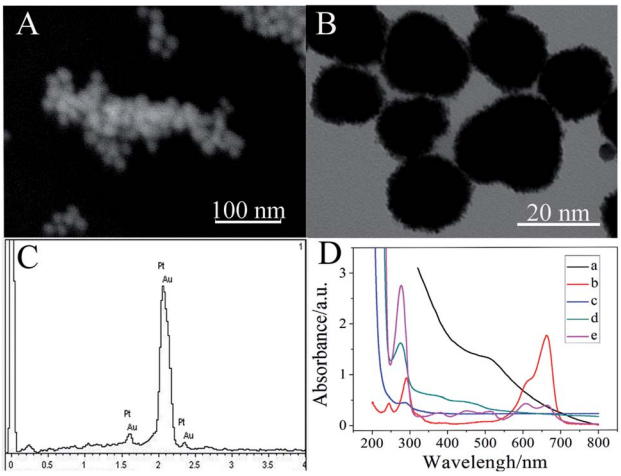

Fig. 2 SEM (A) and TEM (B) images of Au@Pt; (C) EDS of Au@Pt; (D) UV-vis absorption spectra Au@Pt (a), MB (b), $McAb_2$ (c), GOx (d), and GOx/$McAb_2$/MB/Au@Pt (e).

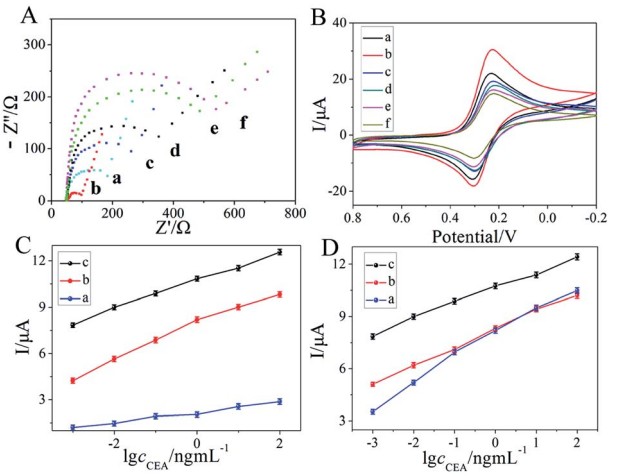

Fig. 3 (A) EIS of bare PWE (a); Au@Pd–PWE (b); $McAb_1$ modified Au@Pd–PWE (c); BSA/$McAb_1$ modified Au@Pd–PWE (d); CEA/BSA/$McAb_1$ modified Au@Pd–PWE (e) and GOx/$McAb_2$/MB/Au@Pt/CEA/BSA/$McAb_1$ modified Au@Pd–PWE (f) in 0.01 M PBS (2.5 mM $[Fe(CN)_6]^{3-/4-}$ containing 0.1 M KCl, pH 7.4). (B) CV at (a) bare PWE, (b) Au@Pd–PWE, (c) $McAb_1$/Au@Pd–PWE, (d) BSA/$McAb_1$/Au@Pd–PWE, (e) CEA/BSA/$McAb_1$/Au@Pd–PWE, and (f) GOx/$McAb_2$/MB/Au@Pt/CEA/BSA/Mc Ab_1/Au@Pd–PWE. (C) EC profiles of the immuosensor using bare PWE (curve a), Au NP modified PWE (curve b), and Au@Pd NP modified PWE (curve c). (D) EC responses of the immuosensor using different signal molecules including GOx/$McAb_2$/MB/Pt (a), GOx/$McAb_2$/MB/Au (b), and GOx/$McAb_2$/MB/Au@Pt (c).

absorption band at around 505 nm was observed for Au@Pt NPs (curve a). The MB has a prominent peak at ~664 nm and a hump at ~614 nm (curve b). Three distinct adsorption peaks from pure GOx were observed (curve d). One adsorption peak at about 276 nm corresponded to the amino acid residues in proteins (the pure GOx and $McAb_2$ (curve c)),[30] and two characteristic absorption peaks of the oxidized form of the pure GOx were located at about 382 and 452 nm respectively. When $McAb_2$ and GOx were linked to MB/Au@Pt, six obvious absorption peaks were observed on the resulting GOx/$McAb_2$/MB/Au@Pt (curve e), indicating successful binding of $McAb_2$ and GOx onto MB/Au@Pt.

3.3 Electrochemical characterization of the μ-PEI

As an available approach to reflect the changes of conducting features of the electrode–electrolyte interface, allowing the understanding of chemical transformation and processes associated with the conductive electrode surface, EIS has been generally employed to characterize the layer-by-layer assembly steps.[31] As shown in Fig. 3A, it was observed that the bare PWE showed a relatively small semicircular domain (curve a). After the growth of an Au@Pd layer, the Au@Pd–PWE showed a lower resistance (curve b), implying that Au@Pd is an excellent electric conducting material and accelerates the electron transfer. Subsequently, the immobilization of $McAb_1$ generated an insulating protein layer (curve c), which increased the resistance. Similarly, the immobilization of BSA, antigens, and signal labels could all resist the electron transfer kinetics of redox probes at the PWE interface. An increased tendency of impedance was observed during their stepwise attachment (curves d–f), which testified to the immobilization of these substances on the PWE surface.

To further confirm the fabrication process of the EC immunosensor, cyclic voltammogram (CV) measurement was employed to characterize the stepwise assembly process in 10.0 mM $[Fe(CN)_6]^{3-/4-}$ solution containing 0.5 M KCl. As shown in Fig. 3B, the bare PWE exhibited one set of well defined redox peaks towards $[Fe(CN)_6]^{3-/4-}$ (curve a). After the growth of an Au@Pd layer, the redox peak currents exhibited an obvious increase, suggesting that Au@Pd–PWE possessed excellent conductivity and a large surface area (curve b). When the Au@Pd–PWE was incubated with $McAb_1$, an obvious decrease in CV response was observed (curve c). Subsequently, the redox peak currents further decreased after the modified PWE was blocked with BSA solution (curve d). Finally, the redox peak currents decreased when incubated with CEA (curve e) and signal labels (curve f). These results were consistent with the fact that this μ-PEI was fabricated as expected.

The modification of the electrode plays an important role in the sensitivity and selectivity of the constructed μ-PEI. As can be seen in Fig. 3C, when the immunodevice was incubated with different concentrations of CEA standard solutions, more obvious increases of EC response appeared from Au@Pd NP modified PWE (curve c) than bare PWE (curve a) and Au NP modified PWE (curve b). The reason may be that the Au@Pd NP modified PWE provided an excellent platform by improving electron transfer and absorbing abundant antibodies.

To clarify the advantage of the developed immunoassay using MB/Au@Pt hybrids, we fabricated different signal labels including GOx/$McAb_2$/MB/Au, GOx/$McAb_2$/MB/Pt, and GOx/$McAb_2$/MB/Au@Pt. The comparison was performed based on the shift of the EC response, when the μ-PEIs were incubated with different concentrations of CEA. As shown in Fig. 3D, the MB/Pt hybrid (curve a) and MB/Au hybrid (curve b) labeled $McAb_2$ performed a lower EC response than that of using MB/Au@Pt hybrid (curve c) labeled $McAb_2$. The MB/Au@Pt hybrid

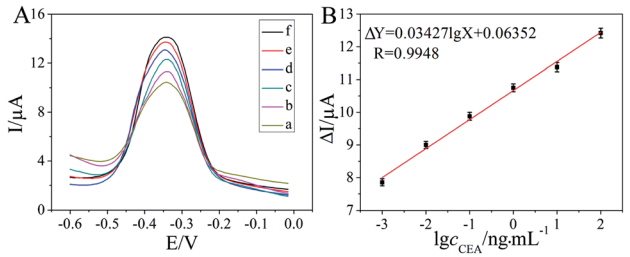

Fig. 4 (A) DPV of the immuosensor in 40 μL of pH 7.4 PBS containing 1.5 mM glucose (under the optimized conditions) with the increase of CEA concentration from (a) to (f) (0.001, 0.01, 0.1, 1, 10, and 100 ng mL^{-1} respectively). (B) Relationship between the DPV peak current and the logarithm of the CEA concentrations.

labeled $McAb_2$ revealed excellent EC performance and 1.5 times signal amplification was obtained compared with other two hybrid labeled $McAb_2$. The reason may be that MB/Au@Pt hybrids had a higher effective EC surface area, good biocompatibility, and facilitated the EC reaction.

3.4 Optimization of detection conditions

The influence of pH on the DPV peak current was investigated in the range from 5.5 to 9.0 (Fig. S2A†). The current intensity increased from 5.5 to 7.4, and the maximum was observed at pH 7.4. Therefore, pH 7.4 electrolyte solution was chosen as the optimal electrolyte solution.

In order to achieve excellent analytical performance of the immunosensor, the effect of the incubation time on the peak current of the immunosensor was investigated between 100 and 220 s. With an increasing incubation time, the DPV peak current increased quickly and reached its maximum value at 170 s (Fig. S2B†). Thus, an incubation time of 170 s was selected in the further study.

3.5 Improvement of Au@Pd–PWE

Under optimized assay conditions, the DPV peak currents were enhanced with the increasing concentration of CEA (Fig. 4A). As shown in Fig. 4B, the calibration plot showed a good linear relationship between the EC response and the logarithm of the analyte concentration in the range from 1.0 pg mL^{-1} to 100 ng mL^{-1}. The limit of detection at a signal-to-noise ratio of 3 was 0.4 pg mL^{-1}. In particular, compared with other immunosensors (Table S1†), the fabricated μ-PEI displayed a wider linear detection range and a lower detection limit.

3.6 Stability, selectivity and reproducibility of the μ-PEI

The stability of the immunosensor, which was evaluated using six concentrations of CEA, is presented in Fig. S3A.† It showed that the DPV current increased with the increase of CEA concentration, and a relative stable curve could be obtained. To investigate the selectivity and specificity of the proposed immunosensor, contrast experiments were performed (Fig. S3B†). Some coexisting species including BSA (100 ng mL^{-1}), casein (100 ng mL^{-1}) and α-1-fetoprotein (AFP) (100 ng mL^{-1}) were used as interfering species to evaluate the selectivity and specificity of the proposed immunosensor. Almost no signal change was obtained compared with the background. The immunosensor was also incubated with concentrations of CEA (1 ng mL^{-1}) containing different interfering species. Compared with the DPV current obtained from the CEA only, no significant difference was found, declaring that hardly any interference generated from those interfering species. Consequently, the good selectivity and specificity of this immunosensor could be confirmed. In addition, the long-term stability of GOx/$McAb_2$/MB/Au@Pt bioconjugates was tested. Due to the biocompatibility of Au@Pt core–shell nanoparticles, GOx/$McAb_2$/MB/Au@Pt bioconjugates could be stored for a long period. When they were stored for 30 days, they retained 94.2% of initial responses. This result showed that GOx/$McAb_2$/MB/Au@Pt bioconjugates exhibited good stability.

3.7 Application in analysis of serum samples

To evaluate the analytical reliability and application potential of the proposed method, the assay results of CEA in human serum samples using the μ-PEI were compared with reference values obtained by the commercially available Electrochemiluminescent (ECL Roche E601, Switzerland) Analyzer as a referenced method. Because of the high sensitivity, serum samples were appropriately diluted with 0.01 M pH 7.4 PBS prior to assay. As shown in Table 1, the assay results have the RSD within 4.34% for CEA detection, indicating feasibility of the proposed method for serum samples.

4 Conclusion

In summary, we reported a sensitive EC immunoanalytical protocol for detection of CEA based on Au@Pd–PWE as a platform and MB/Au@Pt hybrids as signal labels. It was the first time that the modification of PWE on μ-PADs was done through the growth of an Au@Pd alloy NP layer. The Au@Pd–PWE had a

Table 1 Assay results of human serum samples by the proposed and referenced method

Sample no.	Proposed method (ng mL^{-1})[a]	Referenced method (ng mL^{-1})[a]	Relative deviation (%)
1	0.34	0.47	4.34
2	3.22	3.69	−2.78
3	18.2	18.6	−2.1
4	66.5	65.2	2.0

[a] The average value of six successive determinations.

large active surface area and excellent catalytic activity, which played an essential role in not only binding the antibodies, but also assisting the electron transfer process. Improved sensitivity was achieved by using Au@Pt core–shell NPs as carriers. As a consequence, a large amount of MB and GOx could be introduced onto the Au@Pt core–shell NPs. The resulting μ-PEI, with simple, low-cost, ultrahigh sensitivity and satisfactory stability, could be suitable for detection of CEA. In addition, the μ-PEI described here can be easily extended for detection of other cancer biomarkers and has the potential for reliable diagnosis of cancer and other diseases.

Acknowledgements

This work was financially supported by the National Natural Science Foundation of China (21175058 and 21277058) and the Natural Science Foundation of Shandong Province, China (ZR2012BZ002).

Notes and references

1 D. L. Clegg, *Anal. Chem.*, 1950, **22**, 48–59.
2 V. Gubala, L. F. Harris, A. J. Ricco, M. X. Tan and D. E. Williams, *Anal. Chem.*, 2012, **84**, 487–515.
3 S. K. Sia and L. J. Kricka, *Lab Chip*, 2008, **8**, 1988–1991.
4 E. Carrilho, A. W. Martinez and G. M. Whitesides, *Anal. Chem.*, 2009, **81**, 7091–7095.
5 A. W. Martinez, S. T. Phillips, B. J. Wiley, M. Gupta and G. M. Whitesides, *Lab Chip*, 2008, **8**, 2146–2150.
6 A. W. Martinez, S. T. Phillips, G. M. Whitesides and E. Carrilho, *Anal. Chem.*, 2010, **82**, 3–10.
7 W. Zhao, M. M. Ali, S. D. Aguirre, M. A. Brook and Y. Li, *Anal. Chem.*, 2008, **80**, 8431–8437.
8 T. Matsuya, S. Tashiro, N. Hoshino, N. Shibata, Y. Nagasaki and K. Kataoka, *Anal. Chem.*, 2003, **75**, 6124–6132.
9 Z. F. Fu, F. Yan, H. Liu, Z. J. Yang and H. X. Ju, *Biosens. Bioelectron.*, 2008, **23**, 1063–1069.
10 Y. Zhang, W. Y. Liu, S. G. Ge, M. Yan, S. W. Wang, J. H. Yu, N. Q. Li and X. R. Song, *Biosens. Bioelectron.*, 2012, **41**, 684–690.
11 G. S. Lai, H. L. Zhang, T. Tamanna and A. M. Yu, *Anal. Chem.*, 2014, **86**, 1789–1793.
12 X. M. Li, X. Y. Yang and S. S. Zhang, *TrAC, Trends Anal. Chem.*, 2008, **27**, 543–553.
13 L. Q. Qu, L. M. Dai and E. J. Osawa, *J. Am. Chem. Soc.*, 2006, **128**, 5523–5532.
14 G. D. Liu and Y. H. Lin, *J. Am. Chem. Soc.*, 2007, **129**, 10394–10401.
15 D. P. Tang, B. Q. Liu, R. Niessner, P. W. Li and D. Knopp, *Anal. Chem.*, 2013, **85**, 10589–10596.
16 X. Cao, N. Wang, S. Jia, L. Guo and K. Li, *Biosens. Bioelectron.*, 2013, **39**, 226–230.
17 X. Hong, D. S. Wang, R. Yu, H. Yan, Y. Sun, L. He, Z. Q. Niu, Q. Peng and Y. D. Li, *Chem. Commun.*, 2011, **47**, 5160–5162.
18 L. Zhang, J. W. Zhang, Q. Kuang, S. F. Xie, Z. Y. Jiang, Z. X. Xie and L. S. Zheng, *J. Am. Chem. Soc.*, 2011, **133**, 17114–17117.
19 F. Tao, M. E. Grass, Y. Zhang, D. R. Butcher, J. R. Renzas, Z. Liu, J. Y. Chung, B. S. Mun, M. Salmeron and G. A. Somorjai, *Science*, 2008, **322**, 932–934.
20 Y. W. Lee, M. J. Kim, Z. H. Kim and S. W. Han, *J. Am. Chem. Soc.*, 2009, **131**, 17036–17037.
21 X. Cao, Y. Han, C. Z. Gao, X. M. Huang, Y. Xu and N. Wang, *J. Mater. Chem. A*, 2013, **1**, 14904–14909.
22 C. Y. Hu, D. P. Yang, K. Xu, H. M. Cao, B. N. Wu, D. X. Cui and N. Q. Jia, *Anal. Chem.*, 2012, **84**, 10324–10331.
23 R. Pelton, *Trends Anal. Chem.*, 2009, **28**, 925–942.
24 L. Ge, S. M. Wang, X. R. Song, S. G. Ge and J. H. Yu, *Lab Chip*, 2012, **12**, 3150–3158.
25 L. B. Wang, Y. Y. Zhu, L. G. Xu, W. Chen, H. Kuang, L. Q. Liu, A. Agarwal, C. L. Xu and N. A. Kotov, *Angew. Chem., Int. Ed.*, 2010, **49**, 5472–5475.
26 J. X. Yan, L. Ge, X. R. Song, M. Yan, S. G. Ge and J. H. Yu, *Chem.–Eur. J.*, 2012, **18**, 4938–4945.
27 W. P. Li, L. Li, S. G. Ge, X. R. Song, L. Ge, M. Yan and J. H. Yu, *Biosens. Bioelectron.*, 2014, **56**, 167–173.
28 J. Chai, F. Li, Y. Hu, Q. Zhang, D. Han and L. Niu, *J. Mater. Chem.*, 2011, **21**, 17922–17929.
29 H. Wang, Z. Sun, Y. Yang and D. Su, *Nanoscale*, 2013, **5**, 139–142.
30 A. P. Guo, D. Wu, H. M. Ma, Y. Zhang, H. Li, B. Du and Q. Wei, *J. Mater. Chem. B*, 2013, **1**, 4052–4058.
31 R. Cui, C. Liu, J. Shen, D. Gao, J. J. Zhu and H. Y. Chen, *Adv. Funct. Mater.*, 2008, **18**, 2197–2204.

